Water Air Soil Pollut (2019) 230: 115
https://doi.org/10.1007/s11270-019-4157-2

Efficient Removal of Lead from Water Using Stabilized Iron Sulfide Nanoparticles: Effectiveness and Effects of Stabilizer

Yang Zhao · Shuting Tian · Yanyan Gong · Dongye Zhao

Received: 23 October 2018 / Accepted: 12 April 2019 / Published online: 10 May 2019

Abstract Fully stabilized FeS nanoparticles were prepared with water-soluble carboxymethyl cellulose (CMC) as a stabilizer, and investigated for adsorption of lead (Pb^{2+}) ions from simulated drinking water. The optimum particle stabilization was achieved using 0.0025 wt.% of CMC for 50 mg/L FeS (i.e., CMC-to-FeS molar ratio of 0.0005). The particle stabilization technique increased lead removal from 78.1% to 90.3%. However, further increasing the CMC-to-FeS molar ratio to 0.0025 diminished the removal. Rapid adsorption kinetics of Pb by CMC-FeS was observed with an equilibrium time of 240 min. The kinetic data was adequately fitted by a pseudo-second-order kinetic model. The adsorption isotherm showed a sigmoidal S-shape due to complexation of Pb with soluble CMC molecules, and the Sigmoidal isotherm model well fitted the adsorption isotherm data with a maximum monolayer adsorption capacity of 77.0 mg/g. FTIR and XRD analyses indicated that both surface complexation and chemical precipitation (in the form of PbS) were the dominant adsorption mechanisms. Pb uptake was enhanced with increasing CMC-FeS dosage from 10 to 125 mg/L and increasing pH from 4.5 to 8.5. The material can perform well under typical concentrations of a model humic acid (HA) and salts. Yet, unusually high concentrations of HA or hardness ions may exerted elevated inhibitive effect. The findings indicated that CMC-stabilized FeS nanoparticles are promising for effective immobilization of lead in contaminated water and soil.

Keywords Nanoparticle · Iron sulfide · Lead · Heavy metal · Metal immobilization · Adsorption

Y. Zhao · S. Tian · D. Zhao (✉)
Environmental Engineering Program, Department of Civil Engineering, Auburn University, Auburn, AL 36849, USA
e-mail: zhaodon@auburn.edu

Y. Gong (✉)
Guangdong Key Laboratory of Environmental Pollution and Health, School of Environment, Jinan University, Guangzhou 511443 Guangdong, China
e-mail: yanyangong@jnu.edu.cn

1 Introduction

Lead (Pb) is one of the most toxic heavy metals released to water due to increasing industrial activities, such as lead mining, smelting, battery manufacturing, and electroplating. Contamination of drinking water has attracted growing attention following several recent major incidents (e.g., the one in Flint, Michigan, USA) due to its detrimental effects on human blood circulation, kidneys, bones, intestines, liver, nerve, and reproductive systems (Flora et al. 2006; Jaishankar et al. 2014). According to a recent Reuters report (Pell and Schneyer 2016), thousands of U.S. areas are afflicted with lead poisoning; to mitigate human exposure, the United States Environmental Protection Agency (USEPA) has established a maximum contaminant level (MCL) of 15 μg/L for lead in drinking water.

To comply with the stringent water quality regulations, various technologies have been investigated for Pb removal from aqueous solutions, such as chemical

precipitation (Matlock et al. 2002), ion exchange (Maliou et al. 1992), adsorption (Li et al. 2002), membrane filtration (Bessbousse et al. 2008), coagulation-flocculation (Pang et al. 2011), and electrochemical techniques (Liu et al. 2013). Chemical precipitation is often used for treating industrial wastewater of high concentrations of heavy metals, and it is rather costly and can produce large volumes of metal-laden sludge. Ion exchange is more suitable for treating wastewater containing trace levels of heavy metals; however, the process is often too expensive due to resin cost and regeneration issues. Membrane filtration and electrochemical techniques are effective but cost-inhibitive for treating contaminated water and soil (Fu and Wang 2011). Among the treatment processes, adsorption has been considered more practical due to its low cost, simple operation, environmental friendliness, and availability of a variety of adsorbents (Yu et al. 2011; Zhao et al. 2013). Yet, conventional adsorbents such as ion exchangers and metal oxides bear with some serious drawbacks, such as high cost and limited adsorption capacity, especially when the lead concentration is at micrograms per liter level (Fan et al. 2014). Thus, it is of urgent need to explore more cost-effective adsorptive materials with high adsorption affinity and capacity for low concentrations of lead.

Naturally occurring mackinawite (FeS) and synthetic FeS materials have been reported to be effective for adsorption of heavy metals such as Hg, Cu, Cr, and Pb due to their unique molecular structure and surface chemical properties (Gong et al. 2016a, b). For instance, within 5 h, 1 g/L of bio-produced magnetic FeS was able to adsorb 98% of 10 mg/L Pb from water (Ito et al. 2004). Compared with traditional powder or microscale FeS particles, nanoscale FeS materials are expected to offer improved soil deliverability and higher adsorption capacity due to their smaller size, larger specific surface area, more active sorption sites, and higher surface reactivity. Our previous studies demonstrated that carboxymethyl cellulose (CMC), a modified natural polysaccharide, can effectively stabilize FeS particles through concurrent steric hindrance and electrostatic repulsion, forming highly stable FeS nanoparticles (CMC-FeS) with an average particle size of 34 nm. The resultant nanoparticles are not only deliverable into soil but highly effective for immobilizing aqueous Hg via chemical precipitation, ion exchange, and surface complexation with an unusually high adsorption capacity (3449 mg/g) (Gong et al. 2012, 2014). However, to the best of our knowledge, a systematic investigation of CMC-FeS has been lacking on immobilizing Pb at environmentally relevant levels, in particular, at micrograms per liter level, under a variety of solution chemistry conditions.

The overall goal of this study was to test the performance of CMC-FeS for Pb immobilization from aqueous solution. The specific objectives were to (1) prepare various FeS particles with different CMC-to-FeS molar ratios and compare their Pb adsorption effectiveness; (2) examine effects of operation conditions including reaction time, FeS dosage, initial Pb concentration, pH, humic acid (HA), and ionic strength on Pb removal by CMC-FeS nanoparticles; and (3) elucidate the underlying Pb adsorption mechanisms.

2 Experimental Section

2.1 Materials

All chemicals used in this study were analytical grade. Iron sulfate heptahydrate ($FeSO_4 \cdot 7H_2O$), carboxymethyl cellulose (CMC, in the sodium form, molecular weight = 90,000, degree of substitute = 0.7), and HA (sodium salt, 50–60% as humic acid) were obtained from Acros Organics (Morris Plains, NJ, USA). Sodium sulfide nonahydrate ($Na_2S \cdot 9H_2O$), lead chloride ($PbCl_2$), sodium hydroxide (NaOH), sodium chloride (NaCl), and calcium chloride ($CaCl_2$) were purchased from Fisher Scientific (Fair Lawn, NJ, USA).

2.2 Preparation and Characterization of CMC-FeS Nanoparticles

CMC-FeS nanoparticles were synthesized in 200 mL suspensions based on the reaction stoichiometry between Na_2S and $FeSO_4$ in the presence of CMC (Xiong et al. 2009). In brief, under continuous N_2 purging, 1 mL CMC (1%, *w*/*w*) solution, 169 mL DI water, and 20 mL $FeSO_4$ (11.4 mM) solution were mixed in a 250-mL flask to yield a solution with desired concentrations of Fe^{2+} and CMC. Then, a stoichiometric amount of Na_2S (22.8 mM in 10 mL N_2-purged DI water) was added dropwise into the mixture under vacuum and shaking at 150 rpm. The resultant suspension containing 100 mg/L FeS and 0.005 wt.% CMC (i.e., a CMC-to-FeS molar ratio of 0.0005) was sealed under anoxic conditions and aged for 24 h to ensure the full

growth of the nanoparticles. For comparison, non-stabilized FeS particles were prepared without the CMC stabilizer but under otherwise identical conditions.

The chemical compositions and crystallographic structure of the CMC-FeS nanoparticles before and after Pb sorption were performed by X-ray diffractometry (XRD) using a Bruker D8 Discover X-Ray Diffractometer (Bruker Corporation, Billerica, MA, USA). The nanoparticles before Pb adsorption were prepared at 500 mg/L as FeS with a CMC-to-FeS molar ratio of 0.0005 in 500 mL suspension. The Pb-laden nanoparticles were prepared in the presence of 50 mg/L Pb^{2+} and 500 mg/L CMC-FeS at pH 7.0 with an equilibration time of 24 h. To avoid formation of Pb $(OH)_2$ precipitation, the lead stock solution was added successively to the reaction systems as described in Section 2.3. The samples were collected by filtering the suspensions using 25-nm nitrocellulose membrane filters. The solids were then rinsed three times with N_2-purged DI water and subsequently dried at 50 °C for 72 h under N_2 protection using a Precision Economy Incubator (Winchester, VA, USA). The resultant samples were ground into powder and sealed for further analysis. The samples were placed in a zero-background sample holder and scanned from 10° to 80° (2θ angles) with a step interval of 0.01°, a step time of 0.1 s, and a scan speed of 6°/min. The XRD spectra were processed using the MDI Jade 6.5 software loaded with an ICDD database (Materials Dara Inc., Livermore, CA, USA).

Fourier-transform infrared (FTIR) spectroscopy measurements were conducted to investigate interactions between Pb and CMC-FeS. The dried samples were analyzed on a Thermo Scientific Nicolet iS50 FT-IR Spectrometer (Thermo Fisher Scientific, Waltham, MA, USA). For comparison, FTIR spectra for neat CMC and non-stabilized FeS particles were also obtained following the same approach.

The hydrodynamic diameter and zeta potential were analyzed using a Malvern Zetasizer Nano ZS (Malvern Instruments, Worcestershire, UK). It should be noted that for the non-stabilized FeS particles, sonication was performed before analysis to break the aggregates. Solution viscosity was measured using a Gilmont falling ball viscometer (Thermo Fisher Scientific, Waltham, MA, USA) to calibrate the instrument.

2.3 Effects of CMC Concentration on Stability of FeS Nanoparticles and Pb Uptake

To explore the effects of the CMC stabilizer on FeS stability and Pb uptake, FeS particles were prepared at a fixed FeS concentration of 50 mg/L and with various concentrations of CMC (i.e., CMC-to-FeS molar ratios of 0, 0.0002, 0.0004, 0.0005, 0.0008, 0.0010, 0.0015, and 0.0025). The stability of the particles was compared by measuring FeS concentrations in the supernatants following 24 h of gravity settling. To this end, 1 mL of the top 2-cm supernatant was mixed with 1 mL of a 3 M HNO_3 solution to completely dissolve the FeS particles, and then analyzed for total Fe concentrations via ICP-OES 710 ES (Agilent Technologies, Santa Clara, CA, USA).

To investigate the effect of CMC concentration on Pb adsorption, Pb adsorption tests were carried out by treating 5 mg/L of Pb^{2+} with 50 mg/L of FeS particles, which were prepared at various CMC-to-FeS molar ratios, at an initial pH of 7.0. It is noteworthy that the maximum solubility of lead at pH 7.0 was 294 μg/L with a K_{sp} value of $Pb(OH)_2 = 1.43 \times 10^{-20}$ (Gurgel and Gil 2009). To avoid the formation of $Pb(OH)_2$ precipitation, lead stock solution was added successively to the reaction systems so that the solubility would not be exceeded due to the adsorption process. The mixtures were equilibrated for 24 h and then analyzed in the same manner as described in the kinetic tests (Section 2.4).

2.4 Lead Adsorption Kinetic Tests

Batch adsorption kinetic tests were carried out in 30-mL sealed glass bottles under anoxic conditions. The initial CMC-FeS and Pb concentrations were 50 mg/L as FeS (CMC-to-FeS molar ratio of 0.0005) and 250 μg/L, respectively. The pH was kept at 7.0 ± 0.2 during the adsorption through intermittent adjustment using HCl (0.1 M) and/or NaOH (0.1 M). The mixtures were continuously mixed on an end-over-end rotator at 30 rpm at room temperature (20 ± 2 °C). At predetermined time intervals (5, 20, 40, 60, 90, 120, 240, 480, 720, and 1440 min), duplicate vials were sacrificially sampled and filtered through 25-nm membrane filters of nitrocellulose (Millipore Corp., Billerica, MA, USA). The filtrates were then acidified by adding 0.05 mL HNO_3 (1 M) into 5 mL of the sample, and analyzed for aqueous Pb concentrations via ICP-OES 710 ES. The detection limit of Pb was determined to be

5 μg/L at a sample volume of 5 mL. Control tests were carried out in the absence of CMC-FeS under otherwise identical conditions. All tests were duplicated to assure data quality and reproducibility.

2.5 Lead Adsorption Isotherm Tests

Lead adsorption isotherms with CMC-FeS were obtained by running the kinetic tests for 24 h, which was sufficient for the system to reach equilibrium. The experimental conditions were CMC-FeS (CMC-to-FeS molar ratio of 0.0005) = 50 mg/L, initial Pb^{2+} = 500 to 4000 μg/L, and pH = 7.0 ± 0.2. Upon equilibrium, the aqueous Pb concentrations were analyzed following the same procedure as described in Section 2.4. All tests were duplicated to assure data quality and reproducibility.

2.6 Effects of CMC-FeS Dosage, pH, HA, and Ionic Strength

Batch equilibrium adsorption experiments were conducted to determine the effects of CMC-FeS dosage, reaction pH, HA, and ionic strength on Pb^{2+} uptake. The same experimental protocols were followed as in the isotherm tests. To test the effect of CMC-FeS dosage, the initial Pb^{2+} concentration was fixed at 250 μg/L Pb^{2+}, whereas the dosage of CMC-FeS was varied (10, 25, 50, 75, 100, and 125 mg/L). In all cases, the CMC-to-FeS molar ratio was maintained at 0.0005 to assure full stabilization of the nanoparticles and the solution pH was fixed at 7.0 ± 0.2. To investigate the effect of pH, the batch equilibrium adsorption tests were conducted with 50 mg/L of CMC-FeS and 250 μg/L of Pb^{2+} at initial pH values of 4.0, 4.5, 5.0, 5.5, 6.0, 6.5, 7.0, 7.5, 8.0, and 9.0 (the final pH values are provided in respective figure captions). To gauge the effect of HA, the adsorption tests were carried out in the presence of various concentrations of HA (1, 2, 5, and 10 mg/L as total organic carbon (TOC)). To examine the effect of ionic strength, the adsorption tests were performed with various concentrations of NaCl (0, 1, 2, 5, and 10 mM) or $CaCl_2$ (0, 1, 2, 5, and 10 mM). Control tests were conducted without CMC-FeS but under otherwise identical conditions. All tests were duplicated to assure data quality and reproducibility.

3 Results and Discussion

3.1 Effects of CMC Concentration on Particle Stability and Pb Adsorption

The effect of CMC on the stability of FeS particles was tested to determine the critical stabilization concentration (CSC) of the stabilizer, i.e., the minimum CMC needed to fully stabilize the nanoparticles. Upon 24 h of gravity settling, 95% of non-stabilized FeS particles settled out from the supernatant. When the CMC concentration was increased to 0.0025 wt.% (CMC-to-FeS molar ratio = 0.0005) or higher, complete stabilization was achieved, i.e., 100% of the particles remained suspended. The hydrodynamic diameter of the non-stabilized FeS particles (sonicated) was 1154 nm, compared to 144, 203, and 208 nm, for the particles stabilized at a CMC-to-FeS molar ratio of 0.0005, 0.0015, and 0.0025, respectively. Therefore, the CSC was determined to be at a CMC-to-FeS molar ratio of 0.0005.

Figure 1 presents the equilibrium uptake of Pb^{2+} by FeS particles stabilized with various amounts of CMC. Control tests showed that CMC alone cannot remove Pb^{2+} from the aqueous solution. The presence of 50 mg/L non-stabilized FeS immobilized 78.1% of 5000 μg/L Pb^{2+} upon equilibrium. Increasing the CMC-to-FeS molar ratio to 0.0005 enhanced the removal percentage to 90.3%, reaching a peak at the ratio of 0.0005. CMC stabilizes FeS particles via concurrent electrostatic repulsion and steric hindrance, and increasing CMC concentration resulted in smaller FeS particles, and thus greater specific surface area and more sorption sites (Gong et al. 2014). However, further increasing the CMC-to-FeS molar ratio from 0.0005 to 0.0025 progressively decreased Pb^{2+} removal by 13.7%. At elevated surface excess of CMC molecules, a denser CMC coating is formed on the nanoparticles, which limits the access of Pb^{2+} to the particles' surface sites because of blockage of the sorption sites and/or elevated mass transfer resistance (He and Zhao 2008). For the subsequent tests, the optimum CMC-to-FeS molar ratio of 0.0005 was applied considering both physical stability of the FeS particles and Pb removal efficiency.

3.2 Lead Adsorption Kinetics

Figure 2a shows the Pb adsorption kinetics by CMC-FeS. The control tests indicate no significant Pb loss when CMC-FeS was absent. In the presence of the

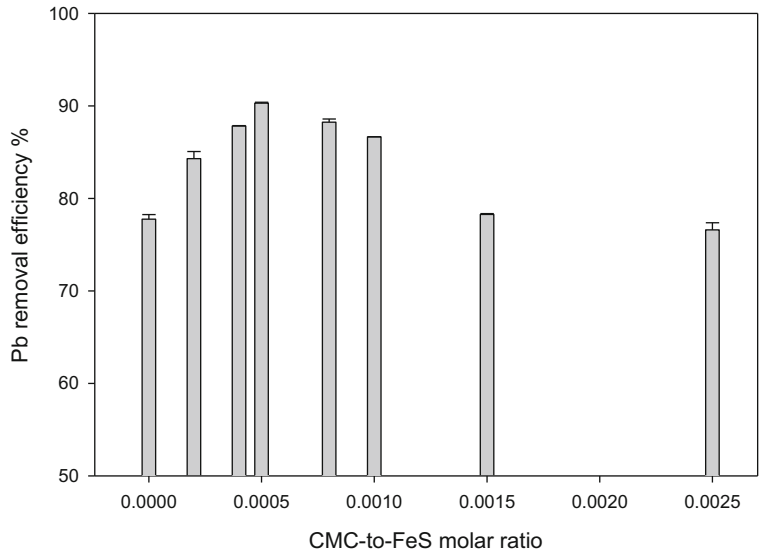

Fig. 1 Equilibrium Pb uptake by FeS particles prepared at various CMC-to-FeS molar ratios. Initial Pb^{2+} = 5 mg/L, FeS = 50 mg/L, and pH = 7.0 ± 0.2. Data plotted as mean of duplicates and error bars (calculated as relative deviation from the mean) indicate data reproducibility

nanoparticles, the aqueous Pb concentration profile showed a rapid initial decrease during the first 120 min (especially the initial 30 min) followed by a gradual stage until equilibrium was reached at 240 min. The phenomenon is consistent with the common notion that more accessible and active sites are taken up first (Liu et al. 2014). The equilibrium Pb concentration in the aqueous phase was 5 μg/L, which is far below the USEPA's MCL for lead in drinking water.

The pseudo-first-order and pseudo-second-order kinetic models were used to interpret the adsorption kinetic data (Fig. 2b) (Liu et al. 2014),

$$\text{Pseudo-first-order kinetic model}: q_t = q_e - q_e \exp(-k_1 t) \quad (1)$$

$$\text{Pseudo-second-order kinetic model}: \frac{t}{q_t} = \frac{1}{k_2 q_e^2} + \frac{t}{q_e} \quad (2)$$

where q_t and q_e (mg/g) are the uptakes of lead at time t (min) and at equilibrium, respectively; and k_1 (min^{-1}) and k_2 (g/(mg·min)) are the respective rate constants. Table 1 gives the resultant model parameters. Overall, the pseudo-second-order kinetic model nearly perfectly fitted the kinetic data with a correlation coefficient (R^2) of 1.000, which suggests that chemisorption may play an important role in lead adsorption by CMC-FeS (He and Zhao 2008).

3.3 Lead Adsorption Isotherms

Figure 3 shows Pb sorption isotherms by CMC-FeS. The classical Langmuir (Liu et al. 2014), Freundlich (Liu et al. 2014), dual-mode (Gong et al. 2014), and sigmoidal (Limousin et al. 2007; Selim and Amacher 1996) isotherm models were tested for fitting the sorption data:

$$\text{Langmuir model}: q_e = \frac{Q_{max} K_L C_e}{1 + K_L C_e} \quad (3)$$

$$\text{Freundlich model}: q_e = K_F C_e^{1/n} \quad (4)$$

$$\text{Dual-mode model}: q_e = K_d C_e + \frac{b Q_{max} C_e}{1 + b C_e} \quad (5)$$

$$\text{Sigmoidal model}: \frac{q_e}{Q_{max}} = \frac{L C_e}{1 + L C_e + \frac{S}{C_e}} \quad (6)$$

where q_e (mg/g) is the equilibrium uptake of Pb, C_e (mg/L) is the aqueous concentration of Pb at equilibrium, and Q_{max} (mg/g) is the monolayer maximum adsorption capacity. For the Langmuir model, K_L (L/mg) represents the Langmuir constant related to the adsorption energy or affinity. For the Freundlich model, K_F (mg/g) is the Freundlich constant related to adsorption capacity, and n is the heterogeneity factor indicating the adsorption intensity of the adsorbate. For the dual-mode model, K_d is the linear distribution coefficient (L/mg), and b is the Langmuir affinity constant (L/mg). For the sigmoidal model, L (L/mg) and S (mg/L) are the sigmoidal

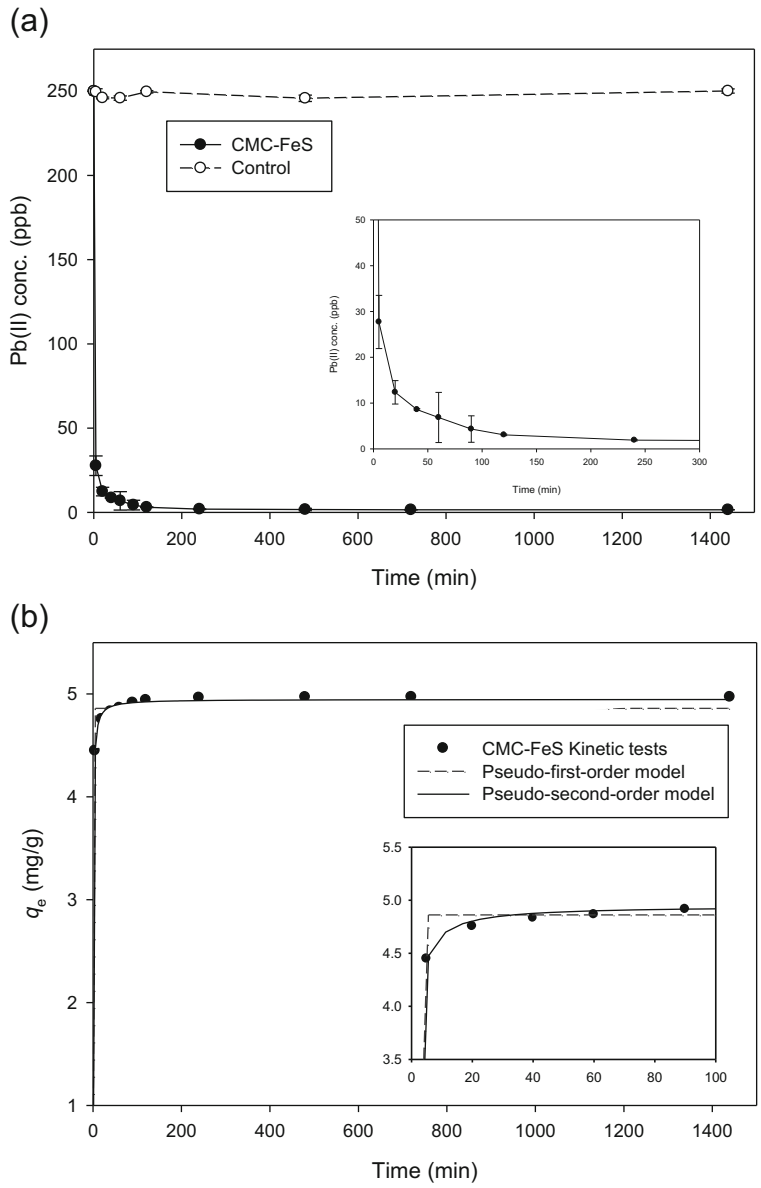

Fig. 2 (**a**) Lead adsorption kinetics by CMC-FeS nanoparticles and (**b**) pseudo-first-order and pseudo-second-order kinetic fittings of the rate data. Symbols: experimental data; lines: model fittings. Experimental conditions: initial Pb^{2+} = 250 μg/L, FeS = 50 mg/L, CMC-to-FeS molar ratio = 0.0005, pH = 7.0 ± 0.2. Data plotted as mean of duplicates and error bars (calculated as standard deviation) indicate data reproducibility

constants related to the adsorption capacity. Table 2 gives the best-fitted model parameters. Evidently, the sigmoidal model outperformed the other three models (R^2 = 0.946, 0.906, 0.817, and 0.906 for sigmoidal, Langmuir, Freundlich, and dual-mode models, respectively).

This sigmoidal S-shape isotherm unveils another important role of CMC. In addition to its particle stabilization effect, CMC acts as a fairly strong ligand to complex with Pb^{2+} through its carboxylate and hydroxyl functional groups (Zhang et al. 2017). On the one hand, the adsorbed CMC molecules on the surface of the FeS nanoparticles can facilitate Pb^{2+} adsorption; on the other hand, CMC molecules in the aqueous phase may form soluble CMC–Pb complexes, which may inhibit the Pb uptake. In the low Pb concentration range, the formation of aqueous CMC–Pb complexes prevented Pb from being effectively taken up by the nanoparticles, resulting in the low Pb uptake. At elevated aqueous Pb concentrations, the complexing capacity of CMC in the aqueous phase was used up, and free Pb species became predominant species, resulting in the sharp rise in the Pb uptake.

Table 1 Pseudo-first-order and pseudo-second-order kinetic models applied for simulating lead sorption kinetic data and the resultant model parameters (errors given as standard deviation)

Kinetic models	Governing equation	Plot equation	Parameters			R^2
Pseudo-first-order	$\frac{dq}{dt} = k_1(q_e - q)$	$q_t = q_e - q_e \exp(-k_1 t)$	k_1 (min^{-1}) 28.361 ± 6.503	q_e (mg/g) 4.907 ± 0.079	$h_1 = k_1 q_e$ (mg/(g min)) 139.17	0.998
Pseudo-second-order	$\frac{dq}{dt} = k_2(q_e - q)^2$	$\frac{t}{q_t} = \frac{1}{k_2 q_e^2} + \frac{t}{q_e}$	k_2 (g/(mg·min) 0.340 ± 0.084	q_e (mg/g) 4.948 ± 0.039	$h_2 = k_2 q_e^2$ (mg/(g min)) 1.68	1.000

The same argument also accounts for the observed CMC effect on Pb uptake (Fig. 1). At the CMC-to-FeS molar ratio below 0.0005, more CMC is adsorbed on the particle surface, facilitating Pb adsorption; conversely, at the CMC-to-FeS molar ratio above 0.0005, more CMC is partitioned in the aqueous phase, resulting in more soluble CMC–Pb complexes and inhibiting the Pb uptake.

CMC-FeS offered much higher monolayer maximum Pb adsorption capacity (Q_{max} = 77.0 mg/g) than other reported adsorbents, such as carbon nanotubes (15.6 mg/g) (Li et al. 2002), tea waste (33.5 mg/g) (Wan et al. 2014), granular activated carbon (15.6 mg/g), and powered activated carbon (26.9 mg/g) (Reddad et al. 2002). Therefore, it can be potentially more effective when used for water treatment or sequestration of Pb in contaminated soil or solid waste.

The chemical (industrial grade) cost for CMC-FeS was estimated to be $1.12/kg, which translates into a material cost of $0.057/$m^3$ of Pb-contaminated water (Pb concentration = 250 μg/L) treated.

3.4 Lead Immobilization Mechanisms

Figure 4 shows the FTIR spectra of bare and CMC-stabilized FeS particles before and after Pb adsorption. The characteristic IR spectra peaks for FeS were reported to be below 400 cm^{-1} (Salavati-Niasari et al. 2010; Chikate and Padhye 2005). The two peaks at 890 and 744 cm^{-1} are due to the Fe–O bonding (Pan et al. 2007). The four peaks observed for CMC-FeS at the wavenumbers of 3137, 1590, 1412, and 1022 cm^{-1} correspond to the interactions between COO^- (1590 and 1412 cm^{-1}) or –OH groups (3137 and 1022 cm^{-1}) and Fe^{2+} (He et al. 2007). The –OH band at 3300 cm^{-1} of CMC shifted to 3137 cm^{-1} for CMC-FeS, which is due to enhanced intermolecular hydrogen bonding between CMC and FeS surface (Sylvestre et al. 2004). The band at 2900 cm^{-1} of neat CMC shifted to 2923 cm^{-1} in CMC-FeS, indicating the C–H stretching vibration from the CH_2 groups of the stabilizer (Maity and Agrawal 2007). The bands at 1590, 1412, and 1022 cm^{-1} are assigned

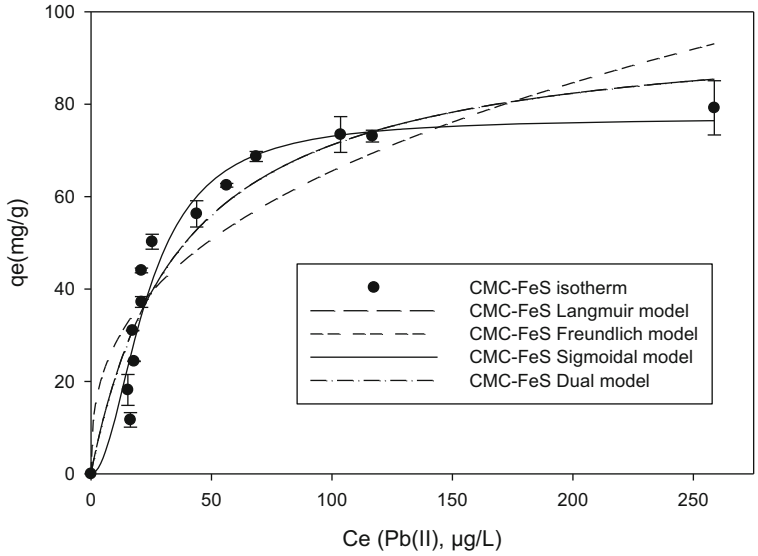

Fig. 3 Adsorption isotherm of Pb by CMC-FeS nanoparticles. Experimental conditions: FeS = 50 mg/L, CMC-to-FeS molar ratio = 0.0005, initial Pb^{2+} = 500–4000 μg/L, and pH = 7.0 ± 0.2. Symbols: experimental data; lines: model fittings. Data plotted as mean of duplicates and error bars indicate data reproducibility

Table 2 Best fitted parameters of Langmuir, Freundlich, Dual-mode, and sigmoidal isotherm models (errors given as standard deviation)

Isotherm model	Parameters			R^2
Langmuir	Q_{max} (mg/g) 97.762 ± 33.617	K_L (L/mg) 0.027 ± 0.022		0.906
Freundlich	K_F (mg/g) 11.968 ± 12.426	n 2.709 ± 4.255		0.817
Dual-mode	Q_{max} (mg/g) 97.762 ± 116.512	b (L/mg) 0.027 ± 0.047	K_d (L/mg) $(2.250 \pm 0.395) \times 10^{-11}$	0.906
Sigmoidal	Q_{max} (mg/g) 77.036 ± 14.094	L (L/mg) $(129.682 \pm 1.218) \times 10^{6}$	S (mg/L) $(708.470 \pm 6.430) \times 10^{8}$	0.946

to asymmetric and symmetric vibrations of the COO^- groups and C–O stretching (RCH_2OH) (Brown et al. 1988). The wavenumber separation (Δ) between the asymmetric $\nu_{as}(COO^-)$ (1590 cm^{-1}) and symmetric $\nu_s(COO^-)$ (1412 cm^{-1}) stretches of CMC-FeS is 178 cm^{-1}, suggesting that bidentate bridging was the primary mechanism for binding CMC to FeS (He et al. 2007; Nakamoto 1977). The FTIR spectra suggested that CMC molecules are adsorbed onto the surface of the nanoparticles via interactions between Fe and the carboxylate and hydroxyl groups. It is also noteworthy that upon CMC loading, the ζ potential of CMC-FeS increased to − 50 mV compared to − 32 mV for the bare FeS. Thus, CMC stabilizes the nanoparticles through concurrent electrostatic repulsion and steric hindrance.

For the Pb-laden bare FeS particles, the two peaks at 890 and 785 cm^{-1} were intensified by 333% and 363% (based on area), respectively, compared to the Pb-free FeS. For CMC-FeS, the Pb loading weakened the peak at 880 cm^{-1} by 94%, but enhanced the peak at 744 cm^{-1} by 1100%. Moreover, the Pb loading increased the IR frequency stretch of O–H (RCH_2OH) at 1022 cm^{-1} by 500%, whereas the peak at 785 cm^{-1} for CMC-FeS disappeared upon Pb loading, while the two peaks at 1590 and 1412 cm^{-1} remained nearly the same before and after the Pb loading. All these observations can be attributed to the surface complexation between CMC-FeS and lead. However, this does not rule out the formation of PbS precipitate because the characteristic absorption band for PbS is at 650 cm^{-1} and is not identifiable from the FTIR spectra (Salavati-Niasari et al. 2010).

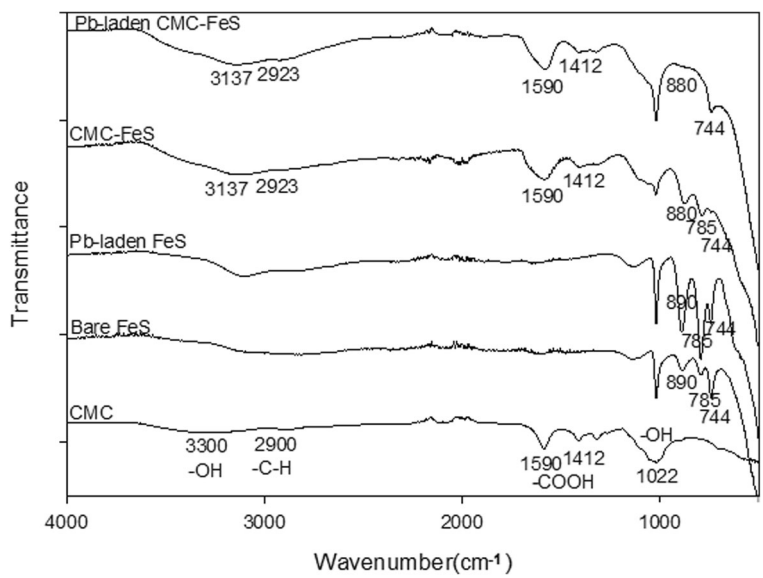

Fig. 4 FTIR spectra of neat CMC powder, non-stabilized FeS particles, CMC-FeS nanoparticles, Pb-laden FeS, and Pb-laden CMC-FeS. Non-stabilized FeS preparation: FeS = 500 mg/L and solution pH = 7.0 ± 0.2; CMC-FeS was prepared at the CMC-to-FeS molar ratio 0.0005 under otherwise identical conditions; Pb-laden FeS and Pb-laden CMC-FeS were prepared by equilibrating the same non-stabilized FeS or CMC-FeS with 50 mg/L of Pb^{2+}

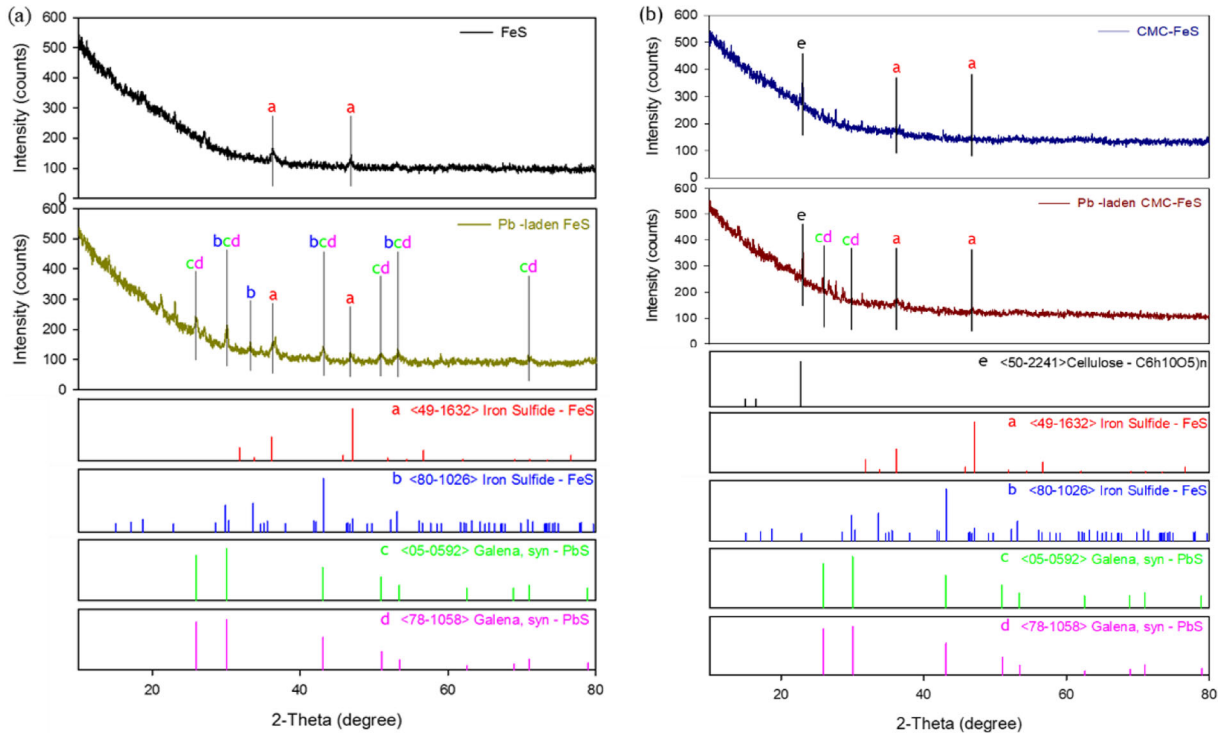

Fig. 5 XRD spectra of (**a**) non-stabilized FeS particles and Pb-laden FeS and (**b**) CMC-FeS nanoparticles and Pb-laden CMC-FeS. Notations: "a" and "b" are the characteristic peaks for FeS, "c" and "d" are the peaks for PbS, and "e" is the characteristic peak for cellulose. Non-stabilized FeS preparation: FeS = 500 mg/L and solution pH = 7.0 ± 0.2; CMC-FeS was prepared at the CMC-to-FeS molar ratio 0.0005 under otherwise identical conditions; Pb-laden FeS and Pb-laden CMC-FeS were prepared by equilibrating the same non-stabilized FeS or CMC-FeS with 50 mg/L of Pb^{2+}

Figure 5 compares the XRD patterns of non-stabilized FeS and CMC-FeS before and after Pb adsorption. For non-stabilized FeS, the peaks at 2θ values of 36.9°and 48.9° were indicative of FeS crystals (ICDD, 49-1632) (Sun et al. 2017; Zhou et al. 2017). Upon Pb^{2+} uptake, these two peaks remained, and in the meanwhile, six new diffraction peaks at 26.1°, 30.1°, 43.1°, 51.0°, 53.7°, and 71.2° appeared, corresponding to the characteristic peaks of galena PbS (ICDD, 05-0592, 78-1058) (Huang et al. 2009). For CMC-FeS, two characteristic peaks of FeS at 36.9° and 48.9° were also observed, plus a new peak at 22.5°, indicating the presence of the CMC stabilizer (Coelho et al. 2016). Upon the Pb loading, two weak peaks at 26.1° and 30.1° were observed, both being attributed to PbS. Regardless of Pb loading, the XRD peaks for CMC-stabilized FeS are much weakened compared to those for non-stabilized FeS. The observation is due to the much smaller particle size of CMC-FeS, and the inhibitive effects of CMC on the growth of FeS and PbS crystals.

Based on the XRD and FTIR spectra, the following reaction mechanisms are proposed for the immobilization of aqueous Pb^{2+} by CMC-FeS:

(a) Chemical precipitation (Skyllberg and Drott 2010):

$$FeS(s) + H^{+} \Leftrightarrow Fe^{2+} + HS^{-} \quad (7)$$

$$Pb^{2+} + HS^{-} \Leftrightarrow PbS(s) + H^{+} \quad \left(K_{sp}(PbS) = 3 \times 10^{-28}\right) \quad (8)$$

$$FeS(s) + Pb^{2+} \Leftrightarrow PbS(s) + Fe^{2+} \quad (9)$$

(b) Surface complexation (Jeong et al. 2007):

$$\equiv FeS(s) + Pb^{2+} \Leftrightarrow \equiv FeS\text{–}Pb^{2+} \quad (10)$$

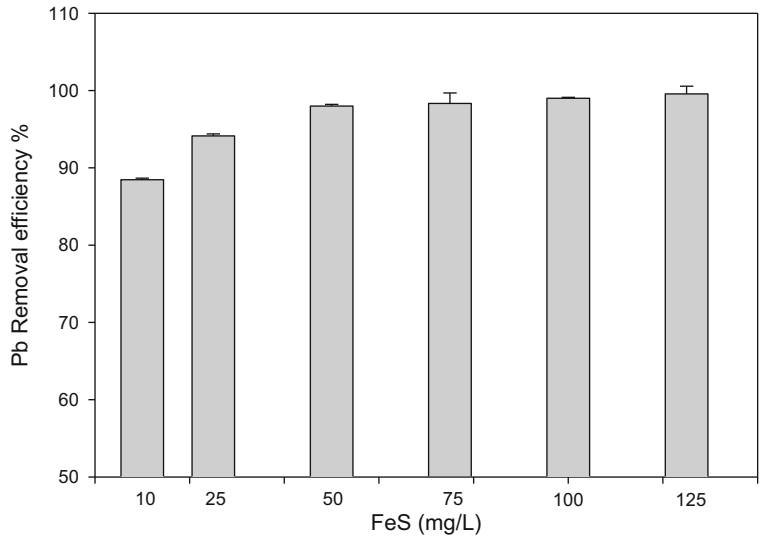

Fig. 6 Effects of CMC-FeS dosage on equilibrium uptake of Pb^{2+} by CMC-FeS. Initial Pb^{2+} = 250 μg/L, CMC-to-FeS molar ratio = 0.0005, and pH = 7.0 ± 0.2. Data plotted as mean of duplicates and error bars (calculated as relative deviation from the mean) indicate data reproducibility

3.5 Effects of CMC-FeS Dosage, pH, HA, and Ionic Strength

Increasing the CMC-FeS dosage from 10 to 50 mg/L enhanced the Pb^{2+} (initial concentration = 250 μg/L) removal efficiency from 88.4% to 98.0% (Fig. 6), which can be attributed to the increase of adsorption sites and chemical precipitation. The removal efficiency remained unchanged when the dosage was further increased from 50 to 125 mg/L. This observation suggests that a small fraction of Pb (< 5 μg/L), which is likely complexed with CMC, is hardly removable.

Removal of Pb by CMC-FeS is pH dependent because pH can affect both particle surface potential and particle stabilization. As the equilibrium pH was increased from 4.5 to 8.5, the Pb removal was elevated from 87.5% to 98.0%, a 10.5% increase (Fig. 7). The pH of the point of zero charge (PZC) of CMC-FeS was < 2.5 (Gong et al. 2012), and thus CMC-FeS was negatively charged over the experimental pH range, and higher pH renders a more negative CMC-FeS surface. Because Pb^{2+} and $Pb(OH)^{+}$ are predominant species in the pH range of 4.5–8.5 (Yang et al. 2010), the higher pH is more conducive to the adsorption of the cationic Pb species. Meanwhile, the increase of pH also gives smaller particles, resulting in larger specific area and more accessible adsorption sites (Gong et al. 2016a, b). In addition, the lower lead adsorption at lower pH can be attributed to the partial dissolution of FeS. As shown in Fig. 7, at pH 4.5, 60% of FeS could be dissolved, while at pH of 6.5 and 8.5, the particle dissolution was reduced to 15% and 6%, respectively.

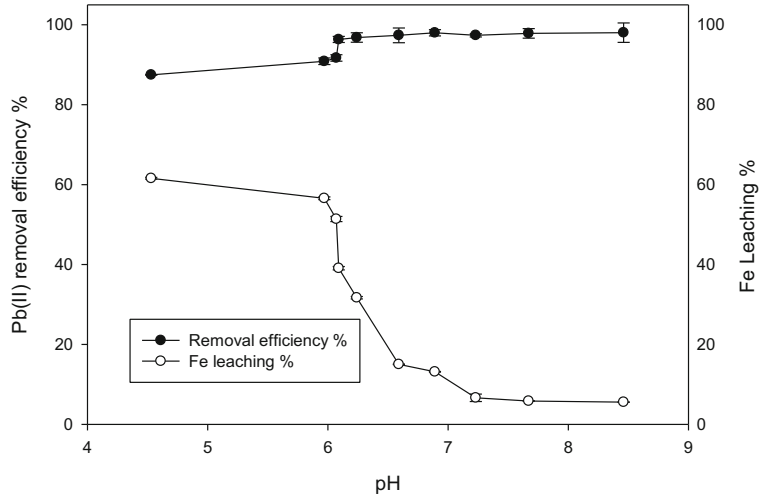

Fig. 7 Effects of equilibrium pH on equilibrium uptake of Pb by CMC-FeS and dissolution of CMC-FeS as a function of pH. FeS = 50 mg/L, CMC-to-FeS molar ratio = 0.0005, and initial Pb^{2+} = 250 μg/L. Data plotted as mean of duplicates and error bars indicate data reproducibility

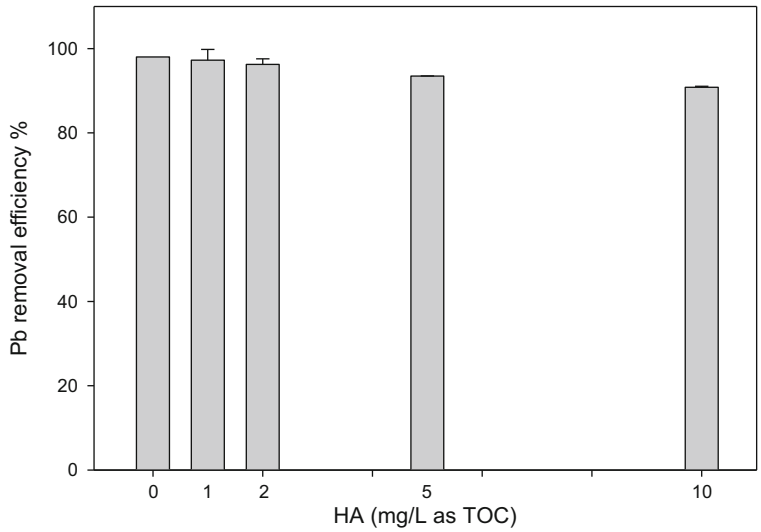

Fig. 8 Effects of HA on equilibrium uptake of Pb by CMC-FeS. FeS = 50 mg/L, CMC-to-FeS molar ratio = 0.0005, initial Pb^{2+} = 250 μg/L, pH = 7.0 ± 0.2. Data plotted as mean of duplicates and error bars (calculated as relative deviation from the mean) indicate data reproducibility

Figure 8 shows the effects of HA on lead removal by CMC-FeS. Increasing the HA from 0 to 10 mg/L (as TOC) decreased the removal efficiency from 98.0% to 90.8%, a 7.2% reduction. However, the presence of 2 mg/L of HA, which is rather common in natural waters, had insignificant effect on the Pb removal. HA can inhibit lead sorption by CMC-FeS in several ways. First, HA can complex with lead in the aqueous phase. HA contains a wide variety of functional groups such as –COOH, –CHO, and $–NH_2$, which may act as electron donors to bind with metals (Baker and Khalili 2004; Zhao et al. 2011). Second, HA can compete with CMC molecules on the surface of CMC-FeS nanoparticles, compromising the stabilization effectiveness of CMC and resulting in larger particles. Third, the uptake of smaller HA molecules on the surface of CMC-FeS increases the mass transfer barrier for Pb uptake.

Figure 9 compares lead uptakes by CMC-FeS in the presence of NaCl and $CaCl_2$ at various concentrations (0–10 mM). It is evident that in the typical concentration range (≤ 2 mM), NaCl and $CaCl_2$ had only modest effect on the Pb removal. Increasing NaCl concentration from 0 to 10 mM suppressed the Pb removal from 98.0% to 90.5%, a 7.5% reduction, whereas increasing the $CaCl_2$ concentration from 0 to 10 mM resulted in a 16.4% decrease in Pb uptake. It is noteworthy that the presence of divalent calcium ions exerted a stronger inhibiting influence on lead adsorption.

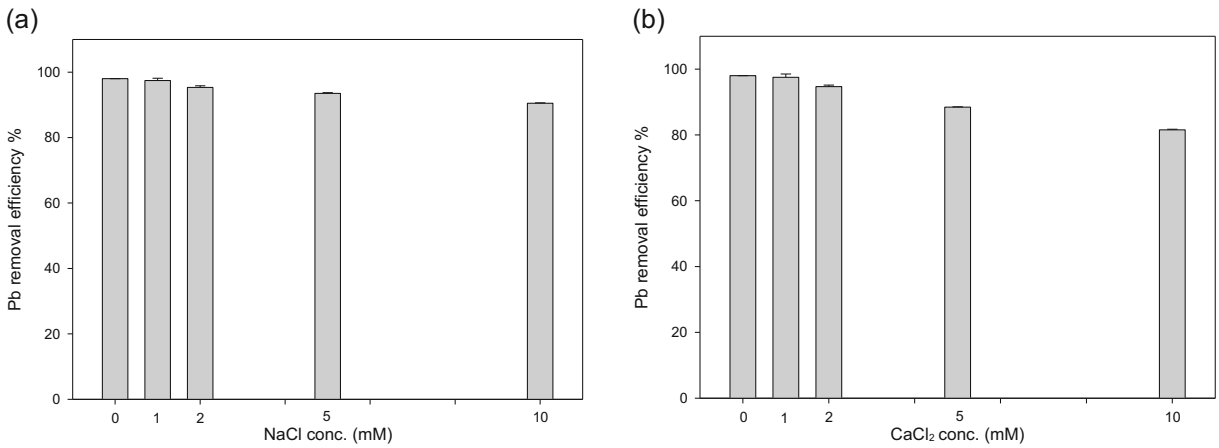

Fig. 9 Effects of coexisting cations (**a**) Na^+ and (**b**) Ca^{2+} on equilibrium adsorption of lead by CMC-FeS. Initial Pb^{2+} = 250 μg/L, FeS = 50 mg/L, CMC-to-FeS molar ratio = 0.0005, pH = 7.0 ± 0.2. Data plotted as mean of duplicates and error bars (calculated as relative deviation from the mean) indicate data reproducibility

Cations may affect lead uptake by CMC-FeS in a number of ways. First, elevated concentrations of Na^+ or Ca^{2+} can compress the electrical double layer of CMC-FeS, and suppress the negative surface potential of the nanoparticles (Gong et al. 2016b), resulting in more aggregation and larger particles. Moreover, the less negative particle surface is less favorable to interactions with the positively charged Pb species. Second, at elevated concentrations, Ca^{2+} and Na^+ ions may directly compete with Pb^{2+} ions for the adsorption sites. And third, Cl^- is an inorganic ligand, which can form soluble $PbCl^+$ and PbOHCl complexes, decreasing the Pb adsorption. As cations of higher valence are more effective in both double-layer compression and competitive ionic pairing, Ca^{2+} ions showed more inhibitive effect on Pb adsorption then Na^+ ions.

4 Conclusions

Lead is considered as one of the most toxic heavy metals in drinking water and the environment. This study demonstrated the potential and viability of CMC-stabilized FeS nanoparticles for enhanced removal of lead from contaminated water or groundwater through a series of batch tests. The main findings are summarized as follows:

1. CMC acted as an effective stabilizer for preparing highly stable FeS nanoparticles. The presence of 0.0025 wt.% CMC fully stabilized 50 mg/L FeS (i.e., a CMC-to-FeS molar ratio of 0.0005) nanoparticles, with a mean hydrodynamic diameter of 144 nm and a zeta potential of − 50 mV.
2. The particle stabilization increased lead removal from 78.1% to 90.3%. However, overdosing of CMC (CMC-to-FeS molar ratio > 0.0005) diminished the lead uptake.
3. Rapid adsorption kinetics of Pb by CMC-FeS was observed with an equilibrium time of 240 min. The kinetic data was adequately fitted by a pseudo-second-order kinetic model.
4. The sigmoidal isotherm model well fitted the adsorption isotherm data with a maximum monolayer adsorption capacity of 77.0 mg/g. FTIR and XRD analyses indicated that both surface complexation and chemical precipitation (in the form of PbS) were the dominant adsorption mechanisms.
5. Pb uptake was enhanced with increasing CMC-FeS dosage from 10 to 125 mg/L and increasing pH from 4.5 to 8.5. The material can perform well under typical concentrations of HA or dissolved organic matter and salts. Yet, unusually high concentrations of HA or hardness ions should be avoided.

The findings in this study indicate that CMC-stabilized FeS nanoparticles hold the potential to be employed as an effective adsorbent for immobilization of lead in contaminated water and soil. In particular, because of the soil deliverability and transportability of stabilized FeS nanoparticles, the material would be useful for in situ or ex situ sequestration of heavy metals in contaminated soil.

Acknowledgments The research was partially supported by the Guangdong Innovative and Entrepreneurial Research Team Program (No. 2016ZT06N569), the National Natural Science Foundation of China (Nos. 41503085 and 41230638), and the Fundamental Research Funds for the Central Universities. The authors would like to gratefully acknowledge Dr. Byron H. Farnum and Ms. Alexandria Combs in the Department of Chemistry and Biochemistry of Auburn University for their assistance with the FTIR analysis, and Mr. Steven Moore in the Material Engineering Program of Auburn University for his help with the XRD operation.

References

Baker, H., & Khalili, F. (2004). Analysis of the removal of lead (II) from aqueous solutions by adsorption onto insolubilized humic acid: temperature and pH dependence. *Analytica Chimica Acta, 516*, 179–186.

Bessbousse, H., Rhlalou, T., Verchère, J. F., & Lebrun, L. (2008). Removal of heavy metal ions from aqueous solutions by filtration with a novel complexing membrane containing poly (ethyleneimine) in a poly (vinyl alcohol) matrix. *Journal of Membrane Science, 307*, 249–259.

Brown, D. W., Floyd, A. J., & Sainsbury, M. (1988). *Organic spectroscopy.* Bath: John Wiley & Sons.

Chikate, R. C., & Padhye, S. B. (2005). Transition metal quinone-thiosemicarbazone complexes 2: magnetism, ESR and redox behavior of iron (II), iron (III), cobalt (II) and copper (II) complexes of 2-thiosemicarbazido-1, 4-naphthoquinone. *Polyhedron, 24*, 1689–1700.

Coelho, C. C. D. S., Cerqueira, M. A. P. R., Albuquerque, P., Silva, O. F., Vicente, A. A., Cabral, L. M. C., & Teixeira, J. A. (2016). Effect of cellulose microcrystals in starch and chitosan-based films properties. In *BioIberoamérica, Book of Abstracts*. Salamanca, Spain, June 5–8, 73, 2016.

Fan, H. T., Sun, X. T., Zhang, Z. G., & Li, W. X. (2014). Selective removal of lead (II) from aqueous solution by an ion-imprinted silica sorbent functionalized with chelating N-donor atoms. *Journal of Chemical & Engineering Data, 59*, 2106–2114.

Flora, S. J., Flora, G., & Saxena, G. (2006). Environmental occurrence, health effects and management of lead poisoning. In *Lead* (pp. 158–228).

Fu, F., & Wang, Q. (2011). Removal of heavy metal ions from wastewaters: a review. *Journal of Environmental Management, 92*(3), 407–418.

Gong, Y., Liu, Y., Xiong, Z., Kaback, D., & Zhao, D. (2012). Immobilization of mercury in field soil and sediment using carboxymethyl cellulose stabilized iron sulfide nanoparticles. *Nanotechnology, 23*, 294007.

Gong, Y., Liu, Y., Xiong, Z., & Zhao, D. (2014). Immobilization of mercury by carboxymethyl cellulose stabilized iron sulfide nanoparticles: reaction mechanisms and effects of stabilizer and water chemistry. *Environmental Science & Technology, 48*, 3986–3994.

Gong, Y., Tang, J., & Zhao, D. (2016a). Application of iron sulfide particles for groundwater and soil remediation: a review. *Water Research, 89*, 309–320.

Gong, Y., Wang, L., Liu, J., Tang, J., & Zhao, D. (2016b). Removal of aqueous perfluorooctanoic acid (PFOA) using starch-stabilized magnetite nanoparticles. *Science of the Total Environment, 562*, 191–200.

Gurgel, L. V. A., & Gil, L. F. (2009). Adsorption of Cu (II), Cd (II) and Pb (II) from aqueous single metal solutions by succinylated twice-mercerized sugarcane bagasse functionalized with triethylenetetramine. *Water Research, 43*, 4479–4488.

He, F., & Zhao, D. (2008). Hydrodechlorination of trichloroethene using stabilized Fe–Pd nanoparticles: reaction mechanism and effects of stabilizers, catalysts and reaction conditions. *Applied Catalysis B: Environmental, 84*, 533–540.

He, F., Zhao, D., Liu, J., & Roberts, C. B. (2007). Stabilization of Fe–Pd nanoparticles with sodium carboxymethyl cellulose for enhanced transport and dechlorination of trichloroethylene in soil and groundwater. *Industrial and Engineering Chemistry Research, 46*, 29–34.

Huang, N. M., Radiman, S., Lim, H. N., Yeong, S. K., Khiew, P. S., Chiu, W. S., & Saeed, G. M. (2009). Synthesis and characterization of ultra small PbS nanorods in sucrose ester microemulsion. *Materials Letters, 63*, 500–503.

Ito, D., Miura, K., Ichimura, T., Ihara, L., & Watanabe, T. (2004). Removal of As, Cd, Hg and Pb ions from solution by adsorption with bacterially-produced magnetic iron sulfide particles using high gradient magnetic separation. *IEEE Transactions on Applied Superconductivity, 14*, 1551–1553.

Jaishankar, M., Tseten, T., Anbalagan, N., Mathew, B. B., & Beeregowda, K. N. (2014). Toxicity, mechanism and health effects of some heavy metals. *Interdisciplinary Toxicology, 7*, 60–72.

Jeong, H. Y., Klaue, B., Blum, J. D., & Hayes, K. F. (2007). Sorption of mercuric ion by synthetic nanocrystalline mackinawite (FeS). *Environmental Science & Technology, 41*, 7699–7705.

Li, Y. H., Wang, S., Wei, J., Zhang, X., Xu, C., Luan, Z. K., Wu, D., & Wei, B. (2002). Lead adsorption on carbon nanotubes. *Chemical Physics Letters, 357*, 263–266.

Limousin, G., Gaudet, J. P., Charlet, L., Szenknect, S., Barthes, V., & Krimissa, M. (2007). Sorption isotherms: a review on physical bases, modeling and measurement. *Applied Geochemistry, 22*, 249–275.

Liu, Y., Yan, J., Yuan, D., Li, Q., & Wu, X. (2013). The study of lead removal from aqueous solution using an electrochemical method with a stainless steel net electrode coated with single wall carbon nanotubes. *Chemical Engineering Journal, 218*, 81–88.

Liu, W., Zhang, P., Borthwick, A. G., Chen, H., & Ni, J. (2014). Adsorption mechanisms of thallium (I) and thallium (III) by titanate nanotubes: ion-exchange and co-precipitation. *Journal of Colloid and Interface Science, 423*, 67–75.

Maity, D., & Agrawal, D. C. (2007). Synthesis of iron oxide nanoparticles under oxidizing environment and their stabilization in aqueous and non-aqueous media. *Journal of Magnetism and Magnetic Materials, 308*, 46–55.

Maliou, E., Malamis, M., & Sakellarides, P. O. (1992). Lead and cadmium removal by ion exchange. *Water Science and Technology, 25*, 133–138.

Matlock, M. M., Howerton, B. S., & Atwood, D. A. (2002). Chemical precipitation of lead from lead battery recycling plant wastewater. *Industrial and Engineering Chemistry Research, 41*, 1579–1582.

Nakamoto, K. (1977). *Infrared and Raman spectra of inorganic and coordination compounds* (3rd edn.). New York: Wiley Interscience.

Pan, B., Liu, X., Ma, S., & Wang, B. (2007). Modifying mg/Al composite catalyst for preparing narrow-range distribution polyether. *Modern Applied Science, 1*, 12.

Pang, F. M., Kumar, P., Teng, T. T., Omar, A. M., & Wasewar, K. L. (2011). Removal of lead, zinc and iron by coagulation-flocculation. *Journal of the Taiwan Institute of Chemical Engineers, 42*, 809–815.

Pell, M. B., & Schneyer, J. (2016). Special Report: Thousands of U.S. areas afflicted with lead poisoning beyond Flint's. Available at https://www.reuters.com/article/us-usa-lead-testing-specialreport/special-report-thousands-of-u-s-areas-afflicted-with-lead-poisoning-beyond-flints-idUSKBN1481BT. Accessed June 2018.

Reddad, Z., Gerente, C., Andres, Y., & Le Cloirec, P. (2002). Adsorption of several metal ions onto a low-cost biosorbent: kinetic and equilibrium studies. *Environmental Science & Technology, 36*, 2067–2073.

Salavati-Niasari, M., Sobhani, A., & Davar, F. (2010). Synthesis of star-shaped PbS nanocrystals using single-source precursor. *Journal of Alloys and Compounds, 507*, 77–83.

Selim, H. M., & Amacher, M. C. (1996). *Reactivity and transport of heavy metals in soils*. New York: CRC Press.

Skyllberg, U., & Drott, A. (2010). Competition between disordered iron sulfide and natural organic matter associated thiols for mercury (II) an EXAFS study. *Environmental Science & Technology, 44*, 1254–1259.

Sun, Y., Lv, D., Zhou, J., Zhou, X., Lou, Z., Baig, S. A., & Xu, X. (2017). Adsorption of mercury (II) from aqueous solutions using FeS and pyrite: a comparative study. *Chemosphere, 185*, 452–461.

Sylvestre, J. P., Kabashin, A. V., Sacher, E., Meunier, M., & Luong, J. H. (2004). Stabilization and size control of gold nanoparticles during laser ablation in aqueous cyclodextrins. *Journal of the American Chemical Society, 126*, 7176–7177.

Wan, S., Ma, Z., Xue, Y., Ma, M., Xu, S., Qian, L., & Zhang, Q. (2014). Sorption of lead (II), cadmium (II), and copper (II) ions from aqueous solutions using tea waste. *Industrial and Engineering Chemistry Research, 53*, 3629–3635.

Xiong, Z., He, F., Zhao, D., & Barnett, M. O. (2009). Immobilization of mercury in sediment using stabilized iron sulfide nanoparticles. *Water Research, 43*, 5171–5179.

Yang, S., Zhao, D., Zhang, H., Lu, S., Chen, L., & Yu, X. (2010). Impact of environmental conditions on the sorption behavior of Pb (II) in Na–bentonite suspensions. *Journal of Hazardous Materials, 183*, 632–640.

Yu, X. Y., Luo, T., Zhang, Y. X., Jia, Y., Zhu, B. J., Fu, X. C., & Huang, X. J. (2011). Adsorption of lead (II) on O_2-plasma-oxidized multiwalled carbon nanotubes: thermodynamics, kinetics, and desorption. *ACS Applied Materials & Interfaces, 3*, 2585–2593.

Zhang, M., He, F., Zhao, D., & Hao, X. (2017). Transport of stabilized iron nanoparticles in porous media: effects of surface and solution chemistry and role of adsorption. *Journal of Hazardous Materials, 322*, 284–291.

Zhao, X., Cai, Y., Wu, F., Pan, Y., Liao, H., & Xu, B. (2011). Determination of perfluorinated compounds in environmental water samples by high-performance liquid chromatography-electrospray tandem mass spectrometry using surfactant-coated Fe_3O_4 magnetic nanoparticles as adsorbents. *Microchemical Journal, 98*, 207–214.

Zhao, X., Hu, B., Ye, J., & Jia, Q. (2013). Preparation, characterization, and application of graphene-zinc oxide composites (G-ZnO) for the adsorption of Cu (II), Pb (II), and Cr (III). *Journal of Chemical & Engineering Data, 58*, 2395–2401.

Zhou, L. H., Wei, X. C., Ma, Z. J., & Mei, B. (2017). Anti-friction performance of FeS nanoparticle synthesized by biological method. *Applied Surface Science, 407*, 21–28.